Current Science
CS 6 (1), 5703-5723 (2026)
Received 08 December 2025 | **Accepted 08 January** 2026 | **Online Available 12 January** 2026
https://doi.org/10.52845/CS/2026-6-1-6

Current Science

Current Science

OPEN ACCESS

ISSN (O) 2795-8639

Original Article

Single Cell Sequencing Dissection of Cellular and Regulatory Networks Driving Arteriovenous Fistula Aneurysmal Dilatation in Hemodialysis

Feng Guo[1], Michael Keese[2], Yu Zhao[1], Yun Wang[3*†], Qining Fu[1*†]

[1]Department of Vascular Surgery, the First Affiliated Hospital of Chongqing Medical University, Chongqing 400016, China

[2]Department of Vascular Surgery, Theresienkrankenhaus, 68165 Mannheim, Germany

[3]Department of Cell Biology, College of Basic Medical Sciences, Army Medical University (Third Military Medical University), Chongqing, 400038, China

†: These Authors Contributed Equally.

***Corresponding Author: Yun Wang, Qining Fu**

Abstract:

Background: Arteriovenous fistula aneurysmal dilatation (AVFAD) is a potentially fatal vascular complication in end-stage renal disease (ESRD) patients undergoing hemodialysis, yet its pathogenic mechanisms remain poorly understood.

Methods: To explore the mechanisms, we applied single-cell RNA sequencing to venous tissues from a Type 1a AVFAD patient (N=1) and a control cephalic vein (N=1) to elucidate pathogenic drivers. In this study, we performed subpopulation composition analysis, pseudotime trajectory analysis, CellChat-based intercellular communication analysis, and transcription factor regulon analysis.

Results: Venous endothelial cells (ECs), smooth muscle cells (SMCs), and neutrophils were examined, indicating ECs dysfunction, synthetic SMCs loss and neutrophils infiltration. Pseudotime analysis revealed dynamic transitions within vascular and immune cell populations. ECs were found to progress from vein 1 and capillaries phenotypes toward lymphatics and arteries. SMCs exhibited a switch from synthetic to contractile phenotype. Additionally, neutrophils transitioned from progenitor subsets marked by $HSP90AA1^{+}$, $IL1B^{+}$, and $ISG15^{+}$ expression to terminally differentiated populations characterized by $RPS18^{+}$ and $S100A12^{+}$ signatures. CellChat analysis uncovered rewiring of ligand-receptor circuits: vein 2/3 subsets in ECs and contractile subset in SMCs dysregulated MTRNR2-FPR2, PECAM1-PECAM1 and ANXA1-FPR1/2 axes to drive neutrophil subsets, while neutrophil autocrine loops (CXCL8-CXCR2, CD55-ADGRE5, and PECAM1-PECAM1) sustained inflammation. High-resolution regulon profiling pinpointed master transcription factors (GATA6+, ZNF76+ in ECs; ZFHX3+, PRDM16+ in SMCs; MBD4+, ZEB1+, KLF16+ in neutrophils) that aligned with these intercellular signals.

Conclusions: Our findings suggest that a neutrophil-vascular axis may drive AVFAD through dynamic cellular reprogramming, offering novel therapeutic targets to mitigate vascular remodeling in hemodialysis patients.

Key words Arteriovenous fistula aneurysmal dilatation; ECs dysfunction; SMCs phenotypic switching; neutrophil infiltration

1. Introduction

End-stage renal disease (ESRD) patients rely heavily on hemodialysis, and arteriovenous fistula (AVF) serves as the standard vascular access [1]. In clinical practice, repetitive puncturing at AVF sites usually leads to vessel-wall injury, promoting neointimal hyperplasia and resulting in

stenosis or thrombosis. However, in a part subset of patients, this trauma can induce progressive degradation of connective tissue fibers that cannot be adequately regenerated given 2-3-day intervals between dialysis sessions, leading to vein wall flaccid and progression to AVF aneurysmal dilatation (AVFAD) [2]. Elevated intraluminal pressure [3] and shear stress from turbulent blood flow [4] further drive this process. The diagnostic threshold for AVFAD is a luminal diameter exceeding 18 mm, with a prevalence of 43.5% [5]. AVFAD is classified into six types: Type 1a (uniform dilation along the vein), Type 1b (immediately distal to the anastomosis), Type 2a (classic "camel-hump"), Type 2b (features of 2a + 1b), Type 3 (complex morphologies), and Type 4 (pseudoaneurysms). Surgical repair is recommended for aneurysm enlargement, overlying skin thinning, ulceration, or other rupture-risk signs. Although emerging data indicate that endothelial-specific blockade of TGF-β reduced collagen deposition and smooth muscle cells (SMCs) proliferation in AVF, thinning the vessel wall [6], and high shear stress promoted endothelial nitric oxide release and MMP-2/9 activation [7], driving excessive extracellular matrix degradation and progressive luminal dilation [8], the cellular and molecular mechanisms underlying AVFAD remain poorly understood, hindered by insufficient bulk-tissue analyses that obscure cell-type-specific effects and intercellular crosstalk.

Single-cell RNA sequencing (scRNA-seq) now offers the resolution needed to dissect heterogeneous cellular dynamics in vascular pathologies, as demonstrated in atherosclerosis [9] and abdominal aortic aneurysms [10], yet it has been only sporadically applied to AVF maturation [11], and rarely to AVFAD. Here, we used 10× Genomics scRNA-seq on Type 1a AVFAD tissue (N = 2, one later excluded), and on paired cephalic vein control to map ECs dysfunction, SMCs phenotypic switching, and neutrophils infiltration. These insights promise to shift therapy from symptomatic management toward targeted preservation of vascular integrity in hemodialysis-dependent patients.

Materials and Methods

Tissues Preparation

Human vascular tissue collection was approved by the Research Ethics Committee of the First Affiliated Hospital of Chongqing Medical University (Approval No. 2025-515-01), with participant recruitment conducted from January 1, 2024, to July 30, 2025. Written informed consent was obtained from all participants. Two venous specimens were obtained from Type 1a AVFAD patients undergoing surgical aneurysmoplasty with stenotic repair. A cephalic vein sample was collected during AVF creation from a patient without prior vascular access. Written informed consent was obtained from all participants in accordance with the Declaration of Helsinki. Immediately after resection, tissues were submerged in preservation solution at 4°C and transported to Shanghai Biotechnology Corporation (China) for 10× Genomics Chromium-based scRNA-seq within 24 hours.

Tissue Dissociation and Single-Cell Suspension Preparation

Tissue was minced into 0.5 mm^3 fragments in ice-cold 1× PBS (RNase-free, Ca^{2+}/Mg^{2+}-free), washed to remove debris, and enzymatically digested in dissociation buffer (0.35% collagenase IV, 2 mg/ml papain, 120 U/ml DNase I) at 37°C for 20 min with gentle agitation. Digestion was quenched with 1× PBS/10% FBS, followed by mechanical dissociation via pipetting. The suspension was filtered through 70 μm and 30 μm strainers, centrifuged (4°C, 300 ×g, 5 min), and treated with MACS lysis buffer (130-094-183, 10×) at room temperature (RT) for 10 min to remove erythrocytes, then centrifuged again (RT, 300 ×g, 5 min). Dead cells were removed using a Miltenyi® Dead Cell Removal Kit (MACS 130-

090-101) , and the pellet was washed twice in 1× PBS/0.04% BSA (4°C, 300 ×g, 3 min). Cell viability (>85%) and concentration (700-1200 cells/μl) were confirmed by trypan blue exclusion and hemocytometry. The final single-cell suspension was loaded onto the 10× Genomics platform for scRNA-seq.

Library Preparation

Cell suspension, reaction mixture (Master Mix + sample), 10× barcoded gel beads (VDJ 3′ Gel Beads v1.1), and partitioning oil were loaded into separate wells of a Chromium Next GEM Chip. Gel bead-in-emulsions (GEMs) were generated via a microfluidic "single-cross" system. Within each GEM, gel beads dissolved to release oligonucleotides that hybridized with reverse transcription (RT) reagents in the Master Mix, producing full-length cDNA tagged with 10× barcodes. After RT, a recovery agent disrupted the oil-water emulsion, and cDNA was purified. Amplified cDNA was fragmented, size- selected, end-repaired, A-tailed, and ligated to Read2 sequencing primers, then P5/P7 adapters were added by PCR to finalize the library.

Data Preprocessing

Raw reads were aligned to *Homo sapiens* genome (GRCh38.p13) and then annotated by CellRanger (https://support.10xgenomics.com/single-cell-vdj) using Ensemble V105 to generate count matrices. Following alignment, cellular barcodes and unique molecular identifiers (UMIs) were analyzed with the Seurat R package (v4.1.0, R v3.6.0). Low-quality cells were filtered out based on mitochondrial UMI content (>25%) or fewer than 500 detected genes per cell. Potential doublets were removed using DoubletFinder (v2.0.4). Post-filtering, the count matrix was normalized via the "LogNormalize" method to mitigate technical variability, and the top 2,000 highly variable features were identified for downstream dimensional reduction.

Dimensionality Reduction and Cell Cluster Identification

Dimensionality reduction was conducted via principal component analysis (PCA), followed by batch-effect correction and data integration using the Harmony algorithm (v1.0) to address technical variability. Subsequent clustering was performed with the Seurat R package (v4.1.0, R v3.6.0) on Harmony-corrected embeddings. Cells were then projected into two dimensions using Uniform Manifold Approximation and Projection (UMAP), where transcriptionally similar populations formed distinct clusters. Differentially expressed genes (DEGs) for each cluster were identified with Seurat's FindAllMarkers function (Wilcoxon rank-sum test), and clusters were annotated using canonical lineage-specific markers, with parameters set to only. pos = FALSE, min.pct = 0.1, and thresh. use = 0.1. Clusters co-expressing markers from divergent lineages were classified as doublets or low-quality cells and excluded from downstream analysis.

Differential Pathway Analysis Across Clinical Groups

DEGs between clinical groups were identified using Seurat FindMarkers with the bimod likelihood ratio test. We applied thresholds of expression in ≥10% of cells in either the target or control subgroup, absolute $\log_2$ fold change ≥0.26, and $p < 0.01$. Gene Ontology (GO) and Kyoto Encyclopedia of Genes and Genomes (KEGG) pathway enrichment analyses were performed with clusterProfiler (v3.16.1), considering Benjamini-Hochberg-adjusted $q < 0.05$ as significant. Gene set variation analysis (GSVA; v1.40.1) was then used to compute pathway activity scores (FDR <0.05), and pathways with adjusted $p < 0.05$ were deemed significantly enriched.

Pseudotemporal Trajectory Analysis

Pseudotemporal trajectory was constructed with the Monocle 2 R package (v2.4.0) using default

parameters. Dimension reduction was performed via the DDRTree method (max components = 2), and cells were ordered in pseudotime. Genes whose expression correlated with pseudotime were identified among the top 50 cluster-specific markers using DifferentialGeneTest (fullModelFormulaStr = ~ Pseudo-time). These dynamic genes were then visualized in a pseudotime heatmap.

CellChat Analysis of Intercellular Communication

Cell-cell communication was analyzed using CellChat (v1.1.3) on the integrated Seurat object. Signaling interactions (paracrine/autocrine) were mapped against CellChatDB. Communication probabilities were calculated using a 20% truncated mean (computeCommunProb; trim = 0.2), followed by network inference and aggregation with default settings. Interaction counts were then visualized to reveal overall network architecture and cluster-specific signaling dynamics.

CellPhoneDB-Based Cell-Cell Interaction Analysis

Cell-type-specific ligand-receptor interactions were systematically analyzed across all subpopulations using CellPhoneDB (v3.1.0, https://www.cellphonedb.org/). Ligand-receptor pairs were considered significant only if they were expressed in >10% of cells within the interacting clusters. CellPhoneDB then performed pairwise comparisons between all cell types and retained only those ligand-receptor pairs with $p < 0.05$.

Transcription Factor Regulation and Downstream Targets Analysis

Transcription factors (TFs) regulatory networks were inferred with pySCENIC (v0.1.1.2) using the RcisTarget motif database and GRNBoost with the default parameters of 50. Each regulatory network was treated as a regulator, and differences in TF activity across cell types were assessed by comparing each network's activity within each population. The specific process: (1) GENIE3 derived TF-target co-expression modules from the scRNA-seq gene expression matrix; (2) RcisTarget identified TF-binding motifs enriched in these modules, producing regulons (TF-target gene sets); (3) AUCell scored regulon activity in each cell to generate an activity matrix; (4) Regulon activation levels were compared across cell types to delineate differential TF regulatory programs. Finally, Sankey diagrams visualized the hierarchical relationships among cell subpopulations, regulons, and their downstream targets.

Results

Single-Cell Profiling and Cell-Type Identification

We collected two venous tissue samples from Type 1a AVFAD patients undergoing aneurysmoplasty with stenotic repair. A control cephalic vein was collected during AVF creation from a patient without prior vascular access. One AVFAD sample was excluded due to insufficient cell yield for scRNA-seq. The overall study design was outlined in Fig. 1A. UMAP visualization of the integrated dataset revealed nine distinct cell types (Fig. 1B), and their relative proportions across samples were shown in Fig. 1C-1D. We noted particularly marked shifts in ECs, neutrophils, and SMCs, which were therefore selected for in-depth follow-up analyses.

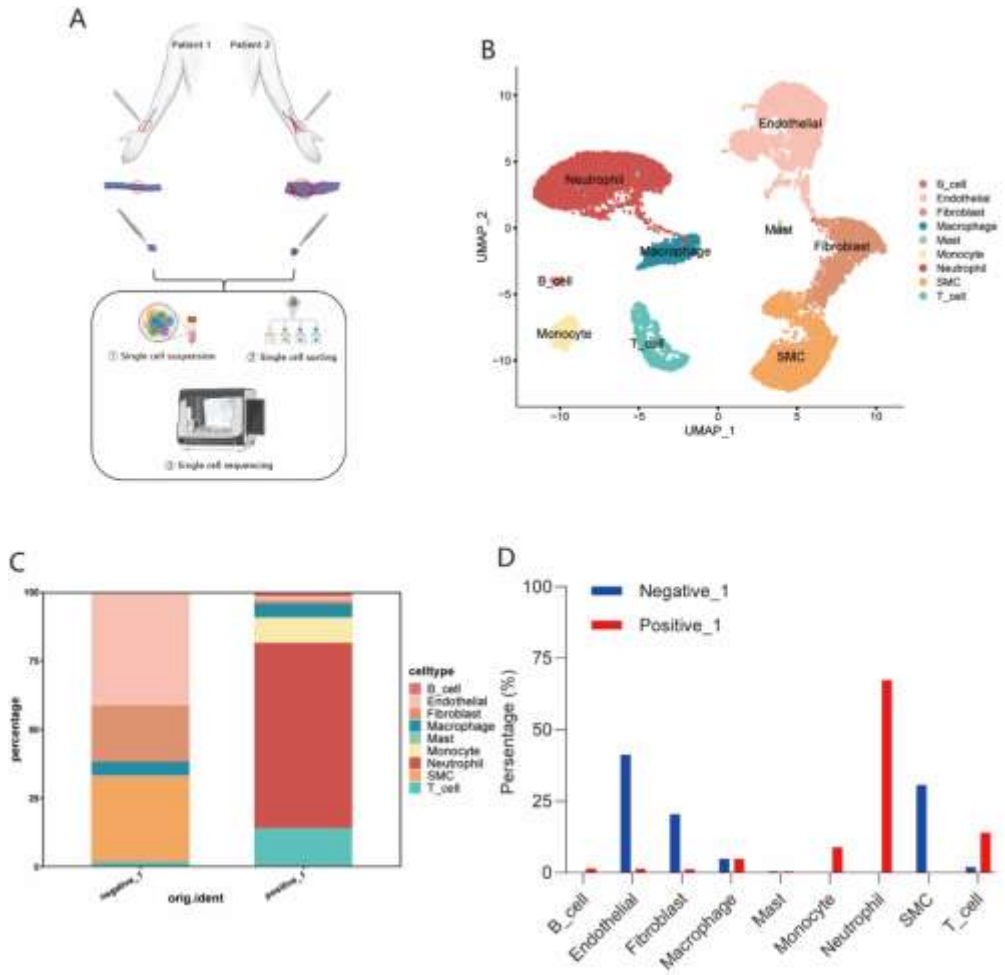

Fig. 1 Single-cell profiling of AVFAD in human tissues. A Study workflow (n=2; patient 1: control; patient 2: AVFAD). B UMAP projection of 22,353 cells grouped into 19 clusters, with major cell types annotated. C-D Relative proportions of major cell categories across sample classifications.

Single-Cell Profiling Identified Cellular Heterogeneity

Building on our initial findings, we performed detailed analyses of ECs, neutrophils, and SMCs. Sub-clustering of ECs revealed seven subpopulations: arteries, capillaries, lymphatics, tip-cells, and three venous subtypes (vein 1-3; Fig. 2A). Comparative quantification across samples showed significant shifts in vein 1-3 abundances (Fig. 2B; Fig. S1A). DEGs profiling of these venous subsets highlighted key signatures (Fig. 2C-2E), with GO/KEGG detailed in Fig. S1B-1G. Neutrophil subclustering resolved five subsets, with a pronounced loss of the RPS18^{+} population in the AVFAD sample (Fig. 2F, G; Fig. S1H); its DEGs and GO/KEGG enrichments are shown in Fig.2H and S1I-1J. Finally, SMCs separated into contractile and synthetic phenotypes (Fig. 2I), with contractile SMCs markedly enriched in AVFAD (Fig. 2J; Fig. S1K) and its DEGs profile depicted in Fig. 2K, with GO/KEGG detailed in Fig. S1L-1M. These findings elucidated specific shifts in ECs, neutrophils, and SMCs subpopulations that drove maladaptive vascular remodeling and AVFAD.

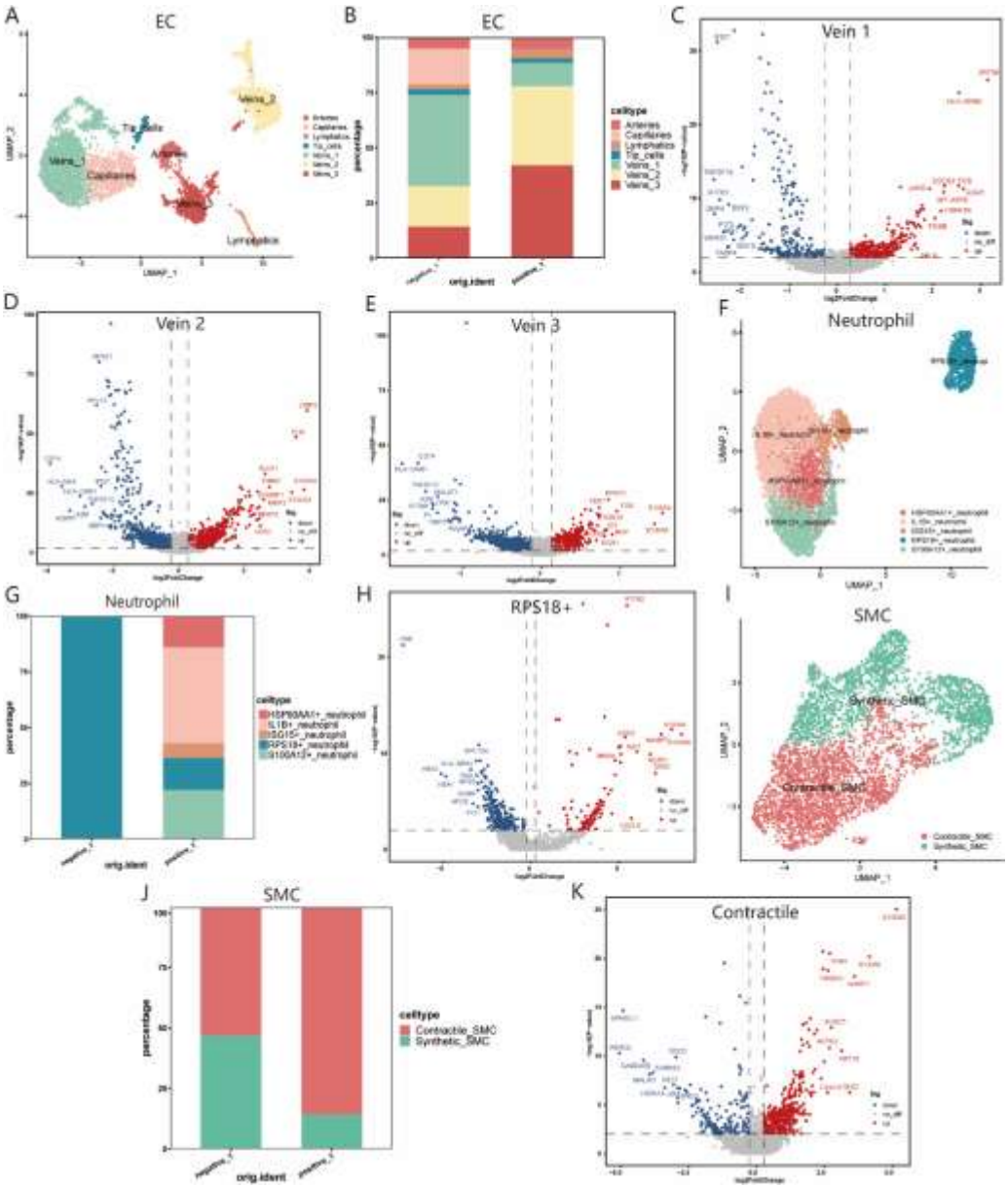

Fig. 2 Subpopulations analysis of ECs, neutrophils, and SMCs. A, F, I UMAP plot of cell subpopulations of each cell type: ECs (12 clusters and 4898 cells), neutrophils (7 clusters and 5402 cells), and SMCs (6 clusters and 4078 cells), respectively. B, G, J Relative proportions of each subpopulation within the respective cell types. Volcano plots showing log_2 fold changes of DEGs in vein 1-3 EC subtypes C-E, $RPS18^+$ neutrophils H, and contractile SMCs K; only genes with adjusted $p < 0.05$ were plotted.

Single-Cell Pseudotemporal Mapping Unveiled Dynamic Cellular Transitions

We reconstructed cell-state trajectories for ECs, neutrophils, and SMCs to trace AVFAD origins. Trajectories colored by samples are shown in Fig. S2A, 2D, 2G, with subpopulations annotations in Fig. S2B, 2E, 2H. In ECs, trajectories initiated in vein 1 and capillaries (darkest blue) and terminated in lymphatics and arteries (lightest blue, Fig. S2C). Here, the start and end points of the pseudotime trajectory from darkest blue to lightest blue were defined by monocle computation. Branch-specific enrichment revealed (Fig. 3A): Branches 1-2: dominated by vein 1 and capillaries; Branch 3: enriched for vein 1-3, capillaries, and tip cells; Branch 4: comprised by vein 1, vein 3, and capillaries; Branch 5:

predominantly vein 2, vein 3, and lymphatics; Branch 6: featured vein 1, vein 2, lymphatics, and arteries. Dynamic gene analysis along these trajectories (Fig. 3B-3C) highlighted ACKR1, CD74, FN1, HLA-DRA, TM4SF1, TXNIP as the most significantly expressed genes. Neutrophils pseudotime trajectories began in HSP90AA1$^+$, IL1B$^+$, and ISG15$^+$ subsets (darkest blue), and ended in RPS18$^+$ and S100A12$^+$ populations (lightest blue, Fig. S2F). Branch analysis (Fig. 3D) showed: Branch 1: HSP90AA1$^+$, IL1B$^+$, and ISG15$^+$; Branch 2: transitional IL1B$^+$, ISG15$^+$, RPS18$^+$, and S100A12$^+$; Branch 3: IL1B$^+$, ISG15$^+$, and S100A12$^+$. Branch 4-5: progressive enrichment of S100A12$^+$ and RPS18$^+$. Key mediators of neutrophil polarization included IGKC, S100A12, S100A4, S100A6, S100A8, and S100A9 (Fig. 3E-3F). SMCs trajectories originated from contractile SMCs (darkest blue), and progressed toward synthetic SMCs (lightest blue, Fig. S2I). Branch 1 was exclusively synthetic SMCs (Fig. 3G), and dynamic gene changes (Fig. 3H-3I) implicated DES, MALAT1, NDUFA4, NEAT1, SORBS2, and STEAP4 in phenotypic switching. Together, these trajectory analyses revealed distinct, state-specific transition in ECs, neutrophils, and SMCs that drove maladaptive remodeling and AVFAD.

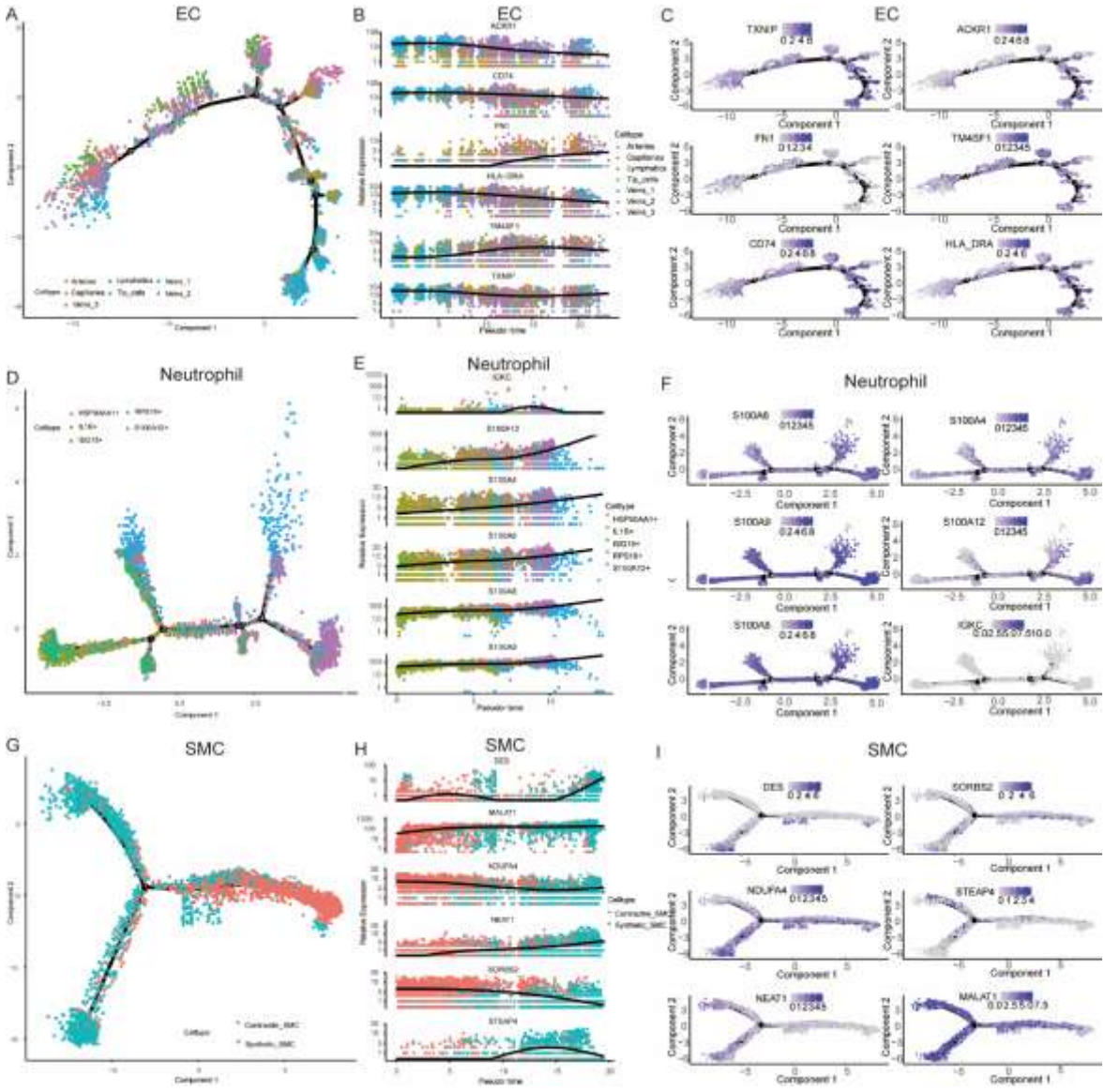

Fig. 3 Pseudotemporal trajectory analysis. A, D, G Trajectory plots of ECs (13 states), neutrophils (11 states), and SMCs (3 states), respectively. B, E, H Expression dynamics of the top six genes across

pseudotime for each cell type, grouped into ECs (9 clusters), neutrophils (7 clusters), and SMCs (6 clusters) respectively (vertical-axis showed relative expression level). C, F, I Overlay of the top six gene expression on the trajectory diagrams, with cells colored by log_2 (UMI + 1) (gray = low, purple = high), illustrating state transitions.

Neutrophil Activation and Vascular Cell Dysregulation in AVFAD Progression Disclosed by Cell-Cell Communication Networks

To delineate AVFAD progression, we mapped intercellular communication networks among ECs, neutrophils, and SMCs. First, we generated a global communication network showing differential interaction counts (colored links) and interaction strengths (link weights) between the three cell types (Fig. 4A-4B; ligand-receptor details in Fig. S3A). In the AVFAD sample, neutrophils exhibited markedly increased outgoing and incoming interaction counts, whereas ECs and SMCs showed significant reductions (Fig. 4C-4D). We then refined our analysis at the subpopulation level, comparing the number of ligand-receptor pairs (Fig. 4E; Fig. S3B) and communication probabilities (Fig. 4F). Consistently, neutrophil subsets displayed elevated interaction counts and probabilities in AVFAD, while EC and SMC subpopulations experienced pronounced declines (Fig. 4G-4H). These findings highlighted enhanced neutrophil activation alongside vascular cell dysregulation as key features of AVFAD progression.

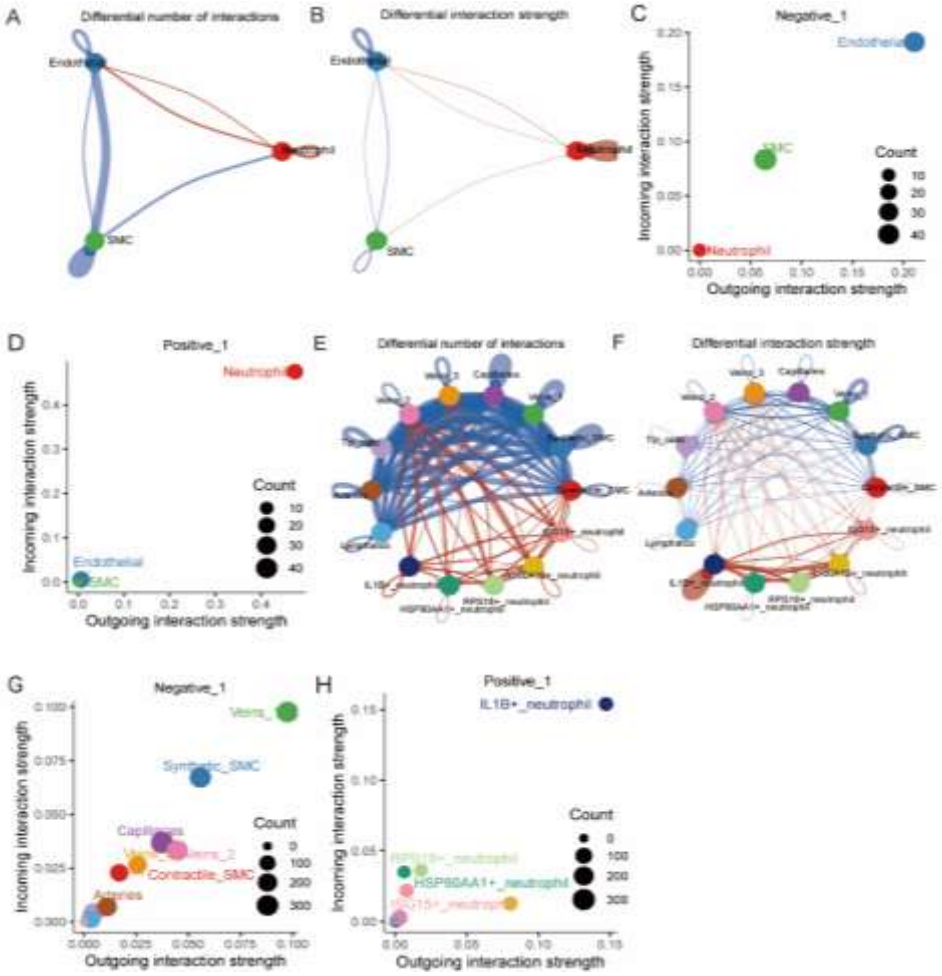

Fig. 4 Cellchat analysis. A-B Circle plots showing intercellular communication networks: colored

nodes represented cell types (node size proportional to cell count), and edges were colored by sender identity with thickness indicating signaling strength. 2D scatter plots comparing outgoing and incoming interaction strengths between negative and positive samples for major cell types C-D and their subpopulations G-H. Circular network diagrams of ligand-receptor pair counts E and communication probabilities F across subpopulations; blue and red lines denoted negative and positive samples respectively, with line thickness reflecting the magnitude of change.

Neutrophil-Vascular Signaling Rewiring in AVFAD Progression Revealed by Subpopulation-Specific Cell-Cell Communication Analysis

Subpopulation-level CellChat analysis revealed dynamic shifts in ligand-receptor signaling during AVFAD progression. In negative sample, vein 1 and capillaries engaged in intra-vein communication via CCL14-ACKR1, PECAM1-PECAM1, APP-CD74, interactions were lost in AVFAD (Fig. 5A, 5D). In AVFAD, vein 2 showed dysregulated ANXA1-FPR1, MTRNR2-FPR2, and PECAM1-PECAM1 signaling with $IL1B^+$, $RPS18^+$, $ISG15^+$ neutrophils, while ANXA1-FPR1 and MTRNR2-FPR2 predominated with $HSP90AA1^+$ and $S100A12^+$ subsets (Fig. 5B). Vein 3 moderately increased ANXA1-FPR1 interactions across all neutrophil subsets (Fig. 5C). Neutrophil subsets interaction loops were also remodeled: $IL1B^+$ cells adjusted CXCL8-CXCR2, CD55-ADGRE5, and PECAM1-PECAM1 signaling, mirrored in $HSP90AA1^+$ (CXCL8-CXCR2) and $RPS18^+$/$ISG15^+$ (CXCL8-CXCR2, PECAM1-PECAM1) neutrophils (Fig. 5E-5G). Contractile SMCs, but not synthetic SMCs, drove neutrophil activation via ANXA1-FPR1/2 axes (Fig. 5H-5I). Network similarity analysis highlighted CXCL, PECAM1, and ANNEXIN pathways as the most disrupted signaling modules in AVFAD (Fig. 5J-5K), underscoring a pathogenic neutrophil-vascular crosstalk.

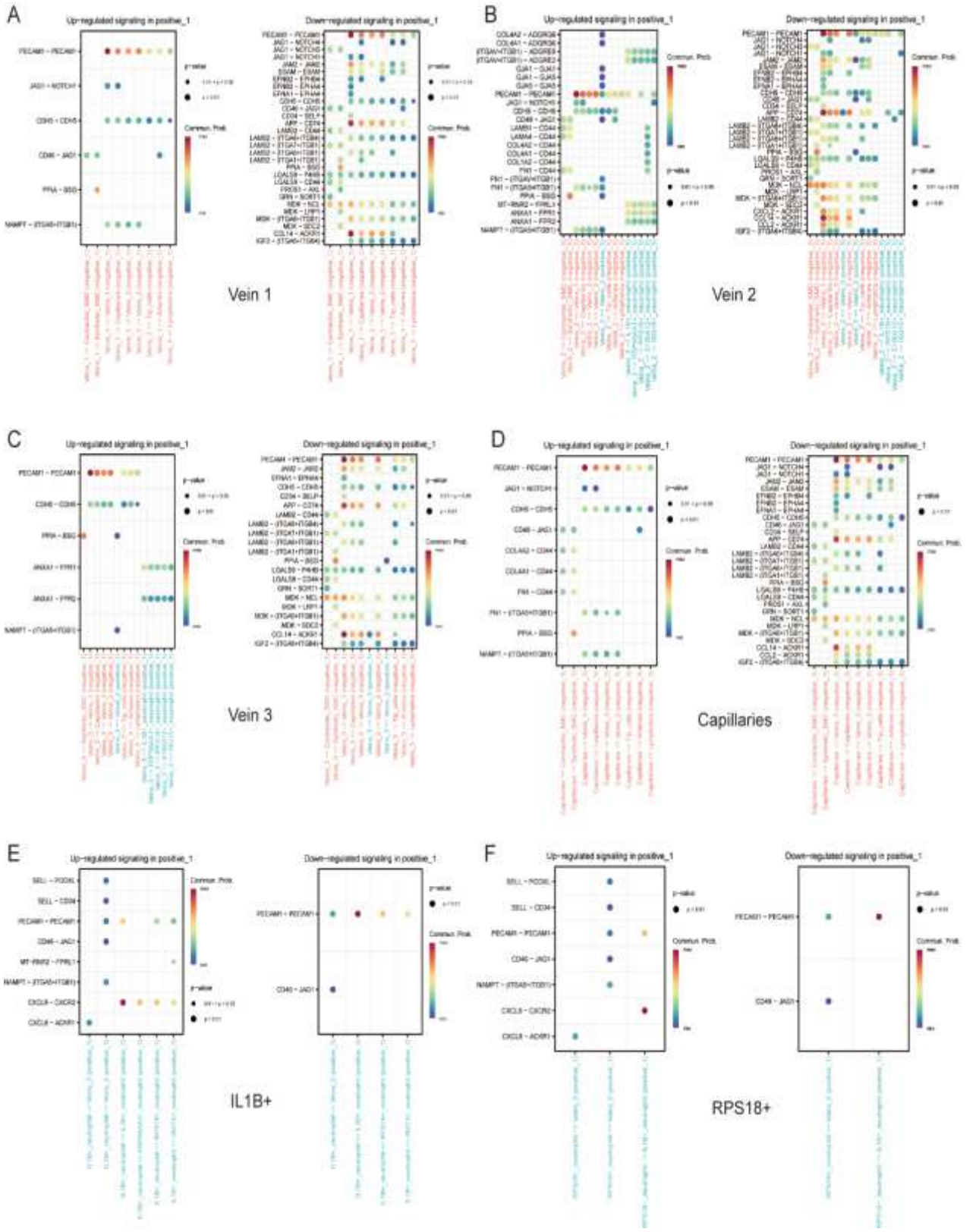
A
Up-regulated signaling in positive_1
Down-regulated signaling in positive_1
Vein 1
B
Up-regulated signaling in positive_1
Down-regulated signaling in positive_1
Vein 2
C
Up-regulated signaling in positive_1
Down-regulated signaling in positive_1
Vein 3
D
Up-regulated signaling in positive_1
Down-regulated signaling in positive_1
Capillaries
E
Up-regulated signaling in positive_1
Down-regulated signaling in positive_1
IL1B+
F
Up-regulated signaling in positive_1
Down-regulated signaling in positive_1
RPS18+

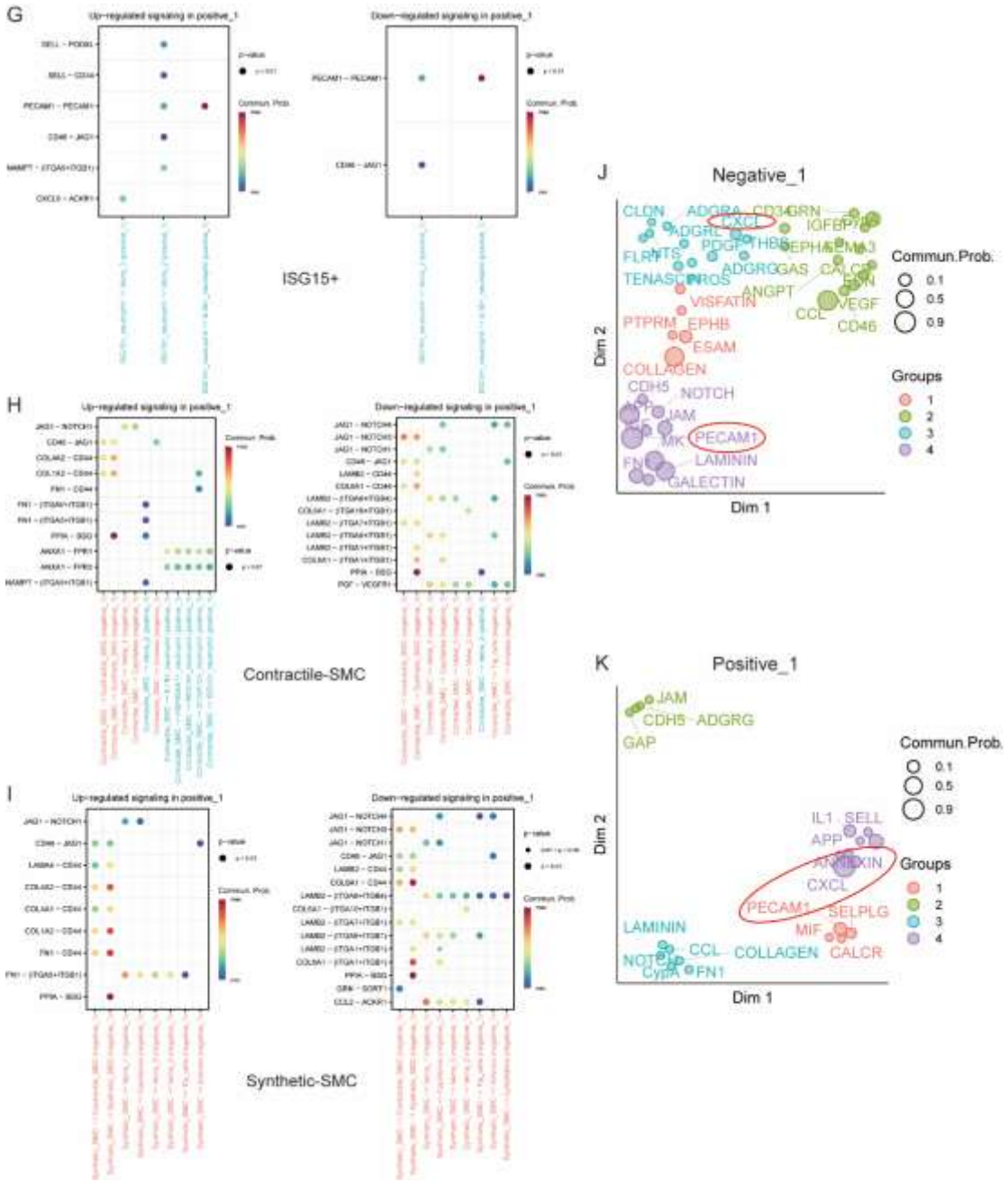

Fig. 5 Dynamics of ligand-receptor interactions. A-I Dysregulated ligand-receptor pairs across cell subpopulations in samples. J-K Signal pathways analysis based on structural similarity: each point represented a pathway, and closer proximity indicated greater network similarity. CXCL and ANNEXIN pathways mediated secreted signaling, whereas PECAM1 mediated cell-cell contact signaling.

Single-Cell Regulon Profiling Uncovered Specific Transcriptional Drives in AVFAD Progression

We next performed systematic regulon analysis in ECs, neutrophils, and SMCs using regulon specificity scores (RSS) and AUC-based activity metrics to pinpoint master TFs. In ECs, 313 regulons were detected across seven subpopulations (vein 1-3, arteries, capillaries, lymphatics, tip cells); the top five regulons (highest RSS) are shown in a heatmap (Fig. S4A). Specifically, the top five regulons in vein 2/3 (Fig. 6A, 6C) exhibited distinct AUC activity

patterns across vascular zones (Fig. 6B, 6D), with the remaining of subsets depicted in Fig. S4B-4K. Among neutrophils, 177 regulons were mapped across five subsets (IL1B^{+}, RPS18^{+}, ISG15^{+}, HSP90AA1^{+}, S100A12^{+}); the top five regulons are depicted in a heatmap (Fig. S4L). Fig. 6E-6J (IL1B^{+}/RPS18^{+}/ISG15^{+}) and Fig. S4M-4P (HSP90AA1^{+}/S100A12^{+}) showed the top 5 regulons and their AUC activity patterns. In SMCs, 299 regulons were detected in contractile and synthetic phenotypes, with the overall top five shown in Fig. S4Q. For contractile SMCs, the top five regulons and their AUC distributions are presented in Fig. 6K-6L, and for synthetic SMCs appear in Fig. S4R-4S. Finally, we traced downstream targets of key regulons (GATA6+, ZNF76+, MBD4+, KLF16+, ZEB1+ and ZFHX3+) using a Sankey diagram to map cell-type-specific regulatory hierarchies (Fig. 7). These regulon-target networks could guide potential therapeutic strategies to prevent AVFAD progression.

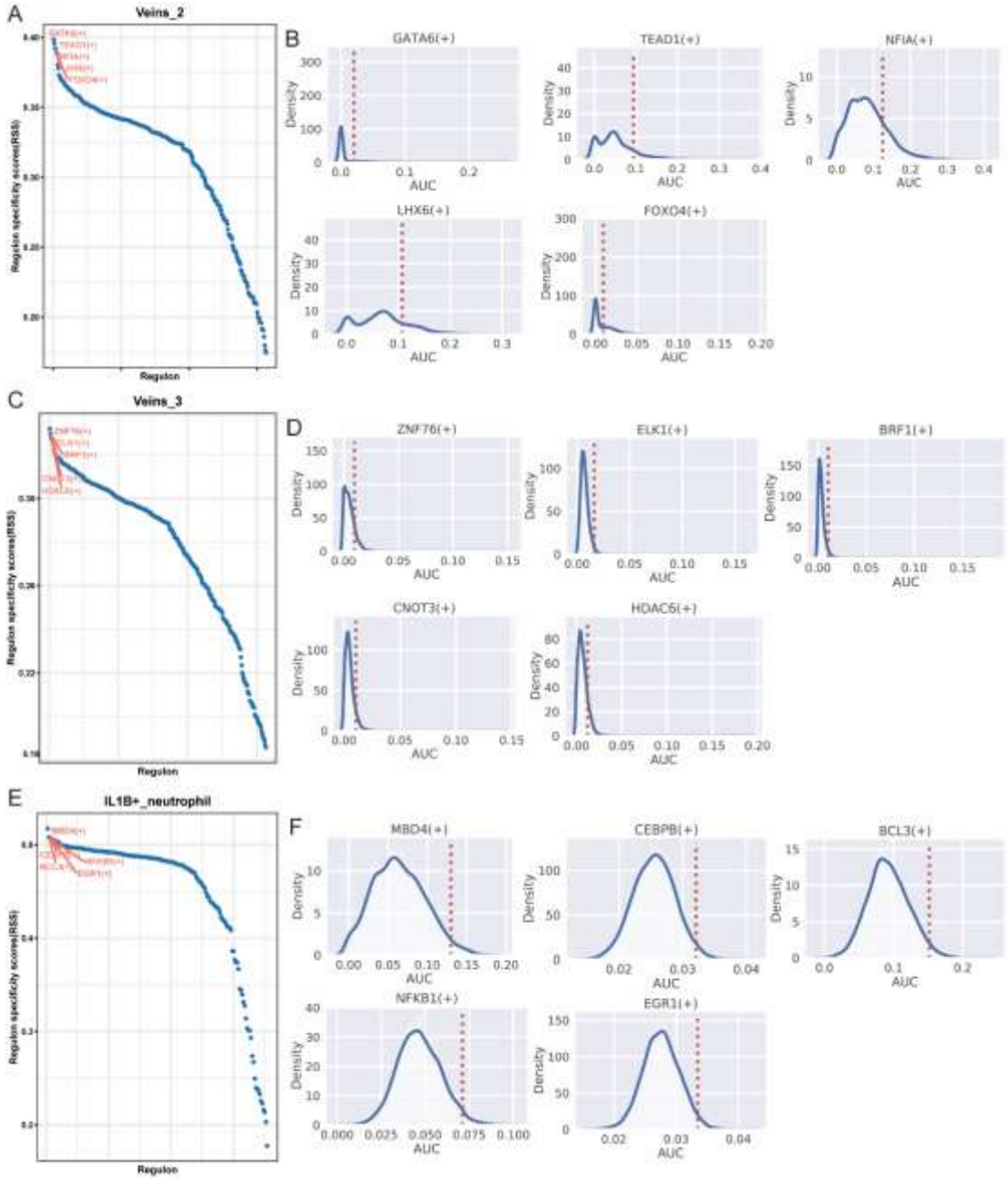

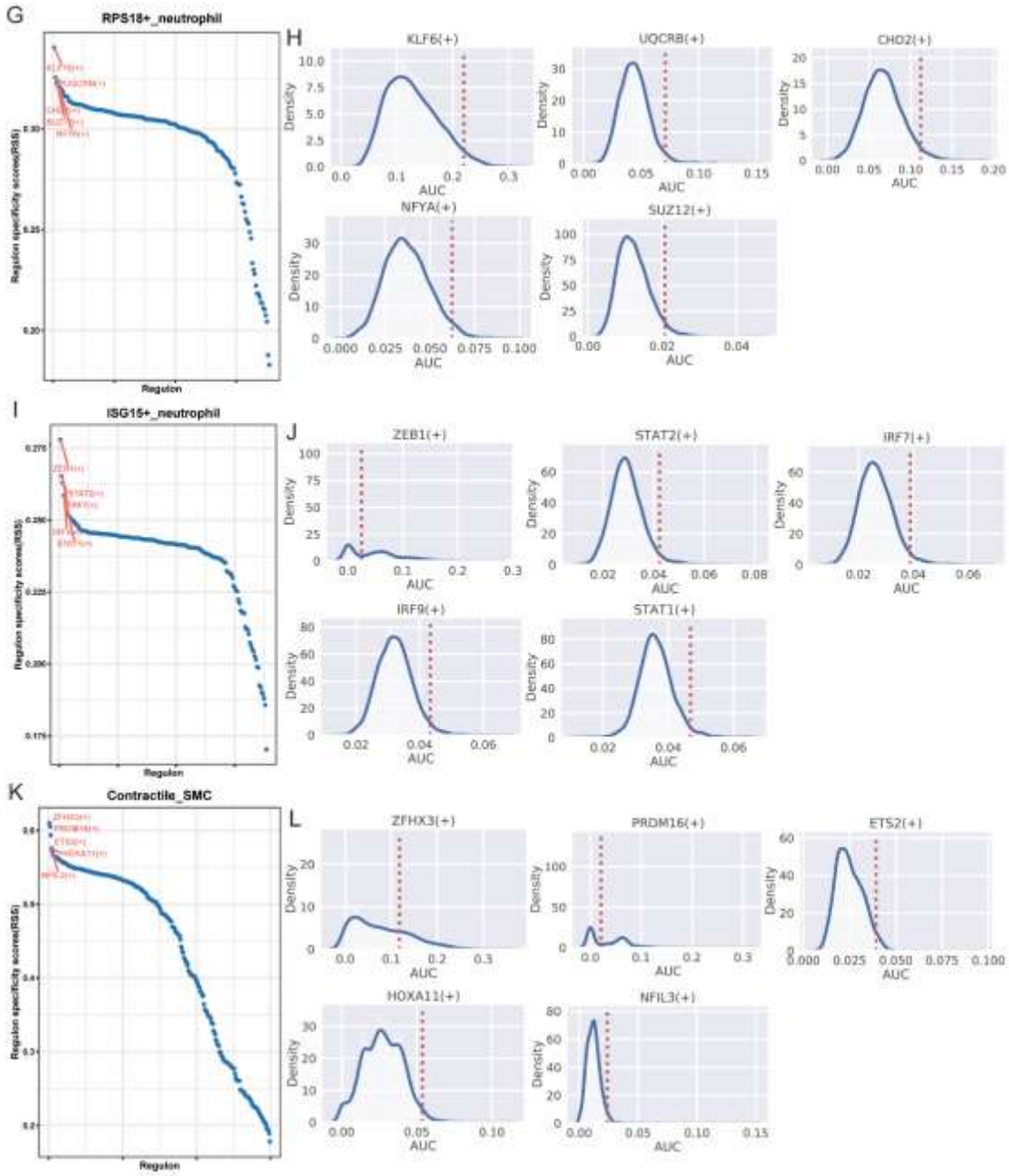

Fig. 6 Regulon analysis. A, C, E, G, I, K Top five regulons by RSS for each subpopulation; the x-axis showed regulon rank, and the y-axis depicted the RSS. B, D, F, H, J, L AUC distributions for each subpopulation; the red line denoted activity threshold. Regulons were considered 'ON' (active/open) in cells with AUC above the threshold and 'OFF' (inactive/closed) otherwise.

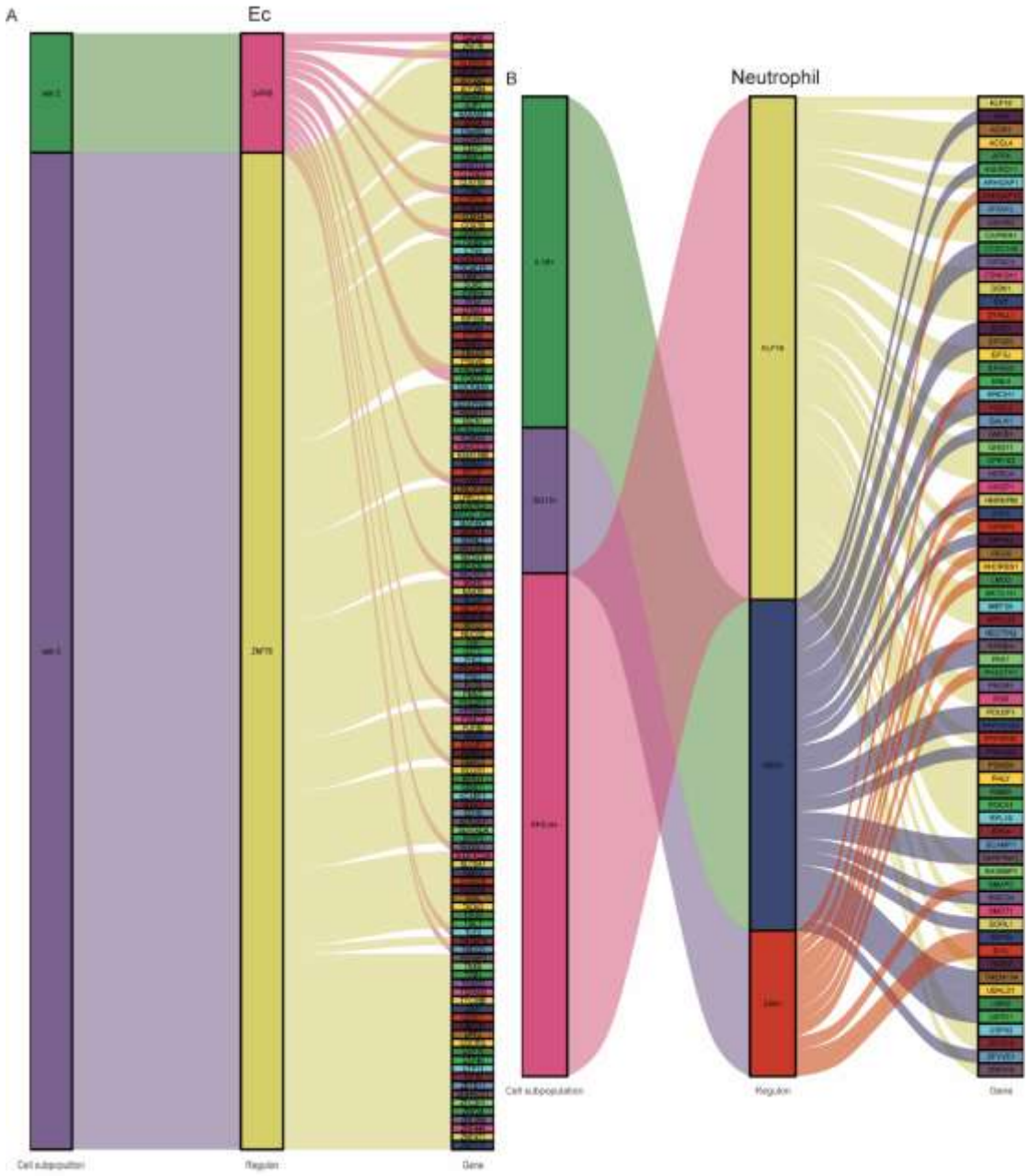
A
Ec
B
Neutrophil

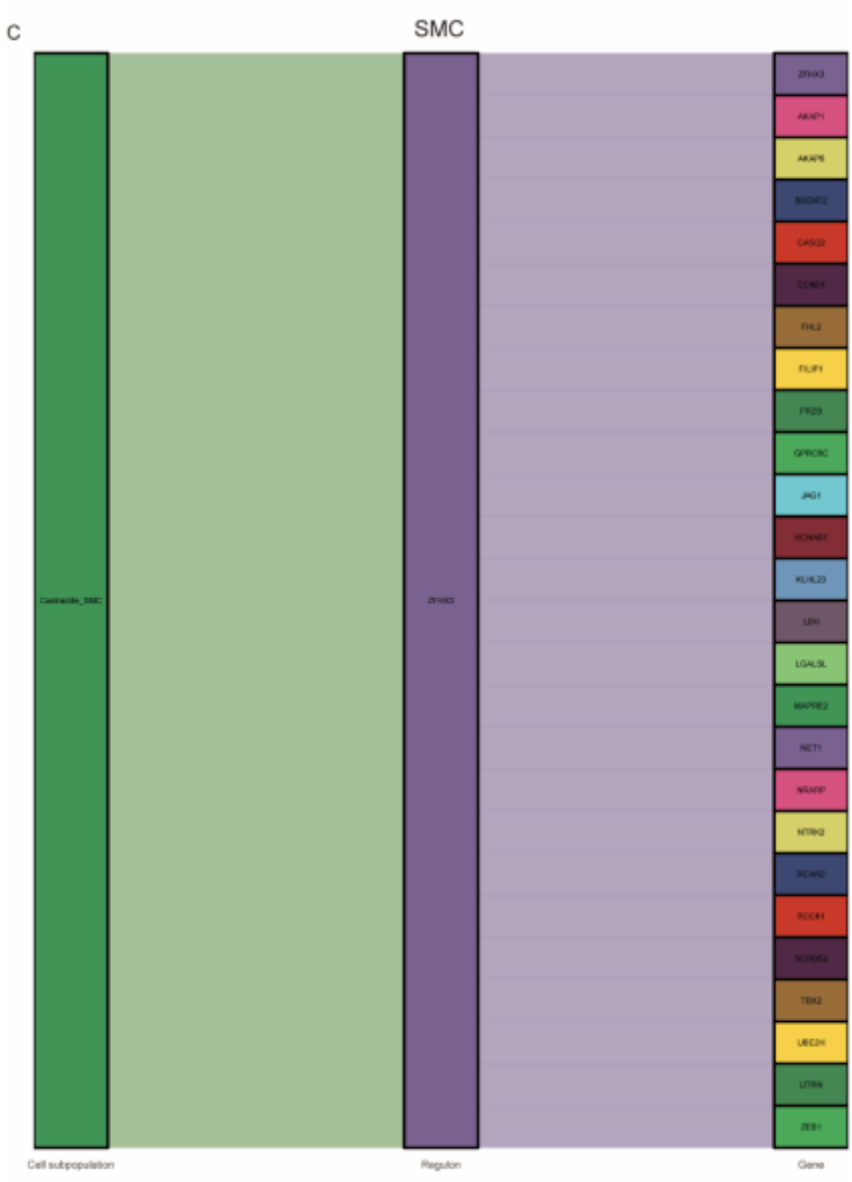

Fig. 7 Target gene-regulon network. The Sankey diagram mapped cell-type-specific regulatory relationships between the identified regulons and their associated target genes.

Discussion

In this study, we applied 10× Genomics scRNA-seq to dissect the cellular and regulatory landscapes underlying AVFAD progression in ESRD patients, revealing three interconnected pathological axes: EC dysfunction, SMC phenotypic switching, and neutrophil-driven inflammation. By comparing Type 1a AVFAD tissue to paired cephalic vein control, our integrative analysis of subpopulation composition, pseudotemporal trajectories, intercellular communication, and TF regulons yielded several novel insights.

Generally speaking, postoperative AVF remodeling progressed through distinct phases: early neointimal hyperplasia and vascular cell proliferation [11], followed within one week by monocyte infiltration, hemostatic gene activation in ECs, and SMCs phenotypic modulation or depletion [12]. By 13 ± 6 weeks, fibroblasts infiltrated the vascular wall, including the intima, indicating chronic stromal remodeling [11]. In AVFAD, we observed a significant reduction in ECs, SMCs, and fibroblasts in aneurysmal tissue,

in contrast to the expansion of fibroblasts during AVF maturation at 13 ± 6 weeks. This depletion of vascular cells, rather than neointimal hyperplasia, suggested maladaptive remodeling that drove vascular-wall thinning. While monocyte infiltration paralleled in early AVF dynamics, AVFAD showed exacerbated immune recruitment dominated by neutrophils and T cells (notably neutrophil subsets: HSP90AA1$^+$, IL1B$^+$, ISG15$^+$, S100A12$^+$), whereas macrophages and B cells remained unchanged. Subpopulation analysis revealed EC dysfunction characterized by a decline in capillaries and vein 1 subsets alongside expansion of vein 2/3, indicating endothelial homeostasis disruption. Concurrently, SMCs underwent a synthetic to contractile phenotypic switch, further contributing to wall thinning. Collectively, these findings underscore ECs, SMCs, and neutrophils as central drivers of AVFAD progression.

We then systematically traced the progression of ECs, SMCs, and neutrophils in AVFAD. Pseudotime trajectory analysis revealed that venous ECs transition from vein 1 and capillaries to lymphatics and arteries, this trajectory was driven by dysregulated genes, including ACKR1, CD74, FN1, HLA-DRA, TM4SF1, and TXNIP. Reports have demonstrated that endothelial cytoskeletal remodeling remained intact without ACKR1 [13] and CD74 exacerbated endothelial injury in vascular disease [14]. FN1 promoted apoptosis and autophagy in vascular ECs under elevated wall tension [15], while TM4SF1-marked endothelial subpopulations became dysregulated under high pressure [16]. TXNIP has also been implicated in pressure-induced endothelial dysfunction [17]. These genes may affect endothelial function in AVFAD, thereby leading to tissue dilatation. Similarly, SMCs underwent a synthetic-to-contractile switch mediated by DES, MALAT1, NDUFA4, NEAT1, SORBS2, and STEAP4, which could drive aneurysmal remodeling. For example, MALAT1 directed SMC phenotypic transitions [18], NEAT1 regulated vascular SMC proliferation, migration, senescence, and phenotypic switching [19], and SORBS2 promoted vascular SMC proliferative and migration [20]. Notable, NEAT1 and SORBS2 were significantly dysregulated in contractile versus synthetic SMCs, suggesting that their roles in weakening vascular vessel-wall integrity. Neutrophil progressed from HSP90AA1$^+$, IL1B$^+$, and ISG15$^+$ progenitor to RPS18$^+$ and S100A12$^+$ terminal subsets. Throughout this differentiation, IGKC, S100A12, S100A4, S100A6, S100A8, and S100A9 emerged as key mediators. IGKC, a B-cell marker [21], remained stably expressed in neutrophils, consistent with our data. Neutrophil-derived S100A12 modulated diverse neutrophil functions [22], and S100A8/A9 orchestrated inflammatory responses [23]. S100A4 and S100A6 also contributed to immune regulation [24], [25], pointing to a coordinated S100-family-mediated control of neutrophil activation in AVFAD.

CellChat analyses then delineated the critical ligand-receptor networks coordinating the pathogenic interactions in AVFAD. EC vein 2/3 subpopulations activated IL1B$^+$, HSP90AA1$^+$, ISG15$^+$, and S100A12$^+$ neutrophil subsets via ANXA1-FPR1, MTRNR2-FPR2, and PECAM1-PECAM1 interactions, engaging the ANNEXIN and PECAM1 pathways. Vein 2 additionally suppressed RPS18$^+$ neutrophils through these same axes, and vein 3 specifically inactivated RPS18$^+$ cells via ANXA1-FPR1. Contractile SMCs similarly activated IL1B$^+$, HSP90AA1$^+$, ISG15$^+$, and S100A12$^+$ neutrophils through ANXA1-FPR1/2-ANNEXIN signaling, while concurrently inhibiting RPS18$^+$ activation. These EC/SMC-neutrophil interactions mirrored the neutrophil abundance shifts seen in AVFAD. Beyond their roles in immune cells, FPR1 [26] and FPR2 [27] expressed on ECs and modulated vascular function. Compound 17b, a small-molecule ANXA1 mimetic, induced vasodilation [28], [29], and enhanced oxidative phosphorylation via

MTRNR2 has been linked to matrix remodeling [30]. PECAM1$^+$ expanded endothelial contact sites, creating highly accessible junctions that facilitated neutrophil transmigration in postcapillary venules [31]. ANXA1 itself was critical for maintaining SMC homeostasis and regulating phenotypic switching [32], and elastase-treated FPR2$^{-/-}$ mice developed aortic dilation with increased neutrophil infiltration and reduced SMC α-actin expression [33]. These observations demonstrated that ECs and SMCs may modulate neutrophil activation through specific ligand-receptor pairs in AVFAD. Remarkably, our analysis uncovered a self-reinforcing inflammatory circuit among neutrophil subpopulations. The IL1B$^+$ subset acted as a bidirectional hub: it activated HSP90AA1$^+$ and ISG15$^+$ neutrophils via CXCL8-CXCR2 and PECAM1-PECAM1, while simultaneously suppressing the RPS18$^+$ subset through the same axes. IL1B$^+$ cells also engaged in autocrine amplification via CXCL8-CXCR2 (CXCL pathway), CD55-ADGRE5 (ADGRE pathway), and PECAM1-PECAM1 (PECAM1 pathway), collectively enhancing their pro-inflammatory activity. Conversely, RPS18$^+$ and ISG15$^+$ subpopulations paradoxically activated IL1B$^+$ cells via reciprocal CXCL8-CXCR2 and PECAM1-PECAM1 signaling, creating a feedforward loop that perpetuated neutrophilic inflammation. Previous study has established that CXCR2 served as a pivotal regulator of neutrophil survival, with CXCL8-mediated activation synergizing potently with macrophage migration inhibitory factor to prolong neutrophil lifespan [34]. Complementing this mechanism, blockade with anti-PECAM-1 antibodies significantly diminished neutrophil infiltration [35]. While CD55-ADGRE5 interactions in neutrophils remained underexplored, emerging evidence indicated that they can modulate immune crosstalk [36] and contribute to tumor immune regulation [37]. Altogether, our integrated cell-cell communication analysis demonstrated that EC/SMC-neutrophil crosstalk and neutrophil auto-stimulation play pivotal roles in initiating aneurysmal dilatation.

We next combined ligand-receptor interaction pattern with high-resolution regulon analysis to further uncover AVFAD pathogenesis. By computing RSS and AUC activity in ECs, neutrophils, and SMCs subpopulations, we identified the top five master regulons aligned with the intercellular signaling programs described above. In vein 2/3, GATA6+ and ZNF76+ emerged as key regulons coordinating ANXA1-FPR1, MTRNR2-FPR2, and PECAM1-PECAM1 signaling to drive neutrophil activation. In contractile SMCs, ZFHX3+ and PRDM16+ ranked highest for stimulating neutrophils, while within the neutrophil auto-stimulation circuit, MBD4+, ZEB1+, and KLF16+ centered the feed-forward loops among IL1B$^+$, RPS18$^+$, and ISG15$^+$ subsets. Few studies have directly linked these regulons to neutrophil function. GATA6+ and ZNF76+, though primarily studied in ECs, mediated monocyte adhesion and migration [38] and regulated macrophage and collagen synthesis [39]. PRDM16 deficiency in the aorta provoked vascular SMC apoptosis and inflammation [40], and its loss in perivascular adipose tissue exacerbated macrophage accumulation and vascular remodeling after injury [41]. ZFHX3 regulated FOXO3 target genes and cell-adhesion pathways [42]. Among our neutrophil regulons, MBD4 loss mediated T cells in systemic sclerosis [43], and increased mortality under chronic inflammation in mice [44]. ZEB1 upregulation via PSMB8-AS1 promoted adhesion-molecule expression and monocyte recruitment [45], while ZEB1 loss impaired both monocytic and neutrophil differentiation [46]. KLF16 correlated with B-cell, CD4$^+$ T-cell, and dendritic-cell infiltration [47]. Although direct effects on neutrophils remained to be proven, these factors likely shaped the AVFAD immune niche. Ultimately, we cataloged the downstream target genes of each regulon, yet

validation was still needed. Our study was limited by small sample size and focused on Type 1a lesions; confirming these findings in larger cohorts and other AVFAD subtypes will be essential. Future work should include perturbation assays, both in vitro and in vivo, to map pathogenic niches within AVFAD.

Conclusions

In summary, our single-cell atlas of AVFAD uncovered a neutrophil-vascular axis in which EC dysfunction, SMC phenotype transition, and neutrophil pro-inflammatory differentiation converged via dysregulated ligand-receptor circuits and master regulons to drive vessel-wall failure. Validation in larger cohorts, including other AVFAD subtypes, and performing perturbation assays will be essential to translate these insights into therapies that preserve AVF integrity in hemodialysis patients.

Acknowledgments We thank the patients for providing tissue samples and Dr. Xia Zhao for performing the surgical procedures.

Supplementary Materials The online supplementary material available at XXXXX.

Author Contributions FG wrote the manuscript and analyzed the data. MK and Y Z; reviewed and edited the manuscript. Y W and QNF provided the concept and supervised this study. All authors have read and agreed to the published version of the manuscript.

Funding This study was sponsored by Natural Science Foundation of Chongqing, China, No. CSTB2023NSCQ-BHX0188.

Data Availability Statement: Single-cell RNA-seq data generated in this study are available in the NCBI Gene Expression Omnibus (GEO) under accession GSE308933. https://www.ncbi.nlm.nih.gov/geo/query/acc.cgi?acc=GSE308933.

Conflicts of Interest The authors declare no conflicts of interest.

Ethics approval and informed consent from participants This study was performed in accordance with the Declaration of Helsinki. The collection of human samples was approved by the Research Ethics Committees of the First Affiliated Hospital of Chongqing Medical University (Approval No. [2025-515-01]). Informed consent was obtained from patients who provided vascular tissues for this study.

References

1. Woodside, K. J., Bell, S., Mukhopadhyay, P., et al., Arteriovenous Fistula Maturation in Prevalent Hemodialysis Patients in the United States: A National Study. *American Journal of Kidney Diseases*, 2018, **71**, 793–801.
2. Yoo, Y. S., Surgical management of a giant venous aneurysm in an autogenous arteriovenous fistula with the vessel loop shoelace technique for wound closure: A case report. *Medicine*, 2021, **100**, e28072.
3. Barac, S., Rata, A. L., Popescu, A. I., Onofrei, R. R., and Chiriac, S. D., True Brachial Artery Aneurysm in Patients with Previous Arterio-Venous Fistula Ligation and Immunosuppressant Therapy for Renal Transplantation: Case Report and Literature Review. *Healthcare*, 2022, **10**, 470.
4. Meola, M., Marciello, A., Di Salle, G., and Petrucci, I., Ultrasound evaluation of access complications: Thrombosis, aneurysms, pseudoaneurysms and infections. *J Vasc Access*, 2021, **22**, 71–83.
5. Valenti, D., Mistry, H., and Stephenson, M., A Novel Classification System for Autogenous Arteriovenous Fistula Aneurysms in Renal Access Patients. *Vasc Endovascular Surg*, 2014, **48**, 491–496.
6. Taniguchi, R., Ohashi, Y., Lee, J. S., et al., Endothelial Cell TGF-β (Transforming Growth Factor-Beta) Signaling Regulates Venous Adaptive Remodeling to Improve Arteriovenous Fistula Patency. *ATVB*, 2022, **42**, 868–883.
7. Tronc, F., Mallat, Z., Lehoux, S., Wassef, M.,

Esposito, B., and Tedgui, A., Role of Matrix Metalloproteinases in Blood Flow–Induced Arterial Enlargement: Interaction With NO. *ATVB*, 2000, **20**.
8. Chan, C.-Y., Chen, Y.-S., Ma, M.-C., and Chen, C.-F., Remodeling of experimental arteriovenous fistula with increased matrix metalloproteinase expression in rats. *Journal of Vascular Surgery*, 2007, **45**, 804–811.
9. Bleckwehl, T., Babler, A., Tebens, M., et al., Encompassing view of spatial and single-cell RNA sequencing renews the role of the microvasculature in human atherosclerosis. *Nat Cardiovasc Res*, 2024, **4**, 26–44.
10. Davis, F. M., Tsoi, L. C., Ma, F., et al., Single-cell Transcriptomics Reveals Dynamic Role of Smooth Muscle Cells and Enrichment of Immune Cell Subsets in Human Abdominal Aortic Aneurysms. *Annals of Surgery*, 2022, **276**, 511–521.
11. Martinez, L., Stoyell-Conti, F. F., Tabbara, M., et al., The Single Cell Landscape of the Human Vein After Arteriovenous Fistula Creation and Implications for Maturation Failure. Molecular Biology, 2025, January 24.
12. Shehadeh, S. A., Tabbara, M., Martinez, L., and Vazquez-Padron, R. I., A snapshot of early venous remodeling in a 7-day-old arteriovenous fistula. *J Vasc Access*, 2023, **24**, 1529–1534.
13. Marchetti, L., Francisco, D., Soldati, S., et al., ACKR1 favors transcellular over paracellular T-cell diapedesis across the blood-brain barrier in neuroinflammation in vitro. *Eur J Immunol*, 2022, **52**, 161–177.
14. Ke, K., Wu, Z., Lin, J., Lin, L., Huang, N., and Yang, W., Increased Expression of CD74 in Atherosclerosis Associated with Inflammatory Responses of Endothelial Cells and Macrophages. *Biochem Genet*, 2024, **62**, 294–310.
15. Wu, H., Liu, K., and Zhang, J., Excess fibronectin 1 participates in pathogenesis of pre-eclampsia by promoting apoptosis and autophagy in vascular endothelial cells. *Molecular Human Reproduction*, 2021, **27**, gaab030.
16. Hong, J., Wong, B., Huynh, C., et al., *Tm4sf1* -marked Endothelial Subpopulation Is Dysregulated in Pulmonary Arterial Hypertension. *Am J Respir Cell Mol Biol*, 2023, **68**, 381–394.
17. Wang, R., Guo, Y., Li, L., et al., Role of thioredoxin-interacting protein in mediating endothelial dysfunction in hypertension. *Genes & Diseases*, 2022, **9**, 753–765.
18. Lyu, L., Li, Z., Wen, Z., et al., Fate mapping RNA-sequencing reveal Malat1 regulates Sca1+ progenitor cells to vascular smooth muscle cells transition in vascular remodeling. *Cell. Mol. Life Sci.*, 2023, **80**, 118.
19. Yin, C., Ge, Z., Yuan, J., et al., NEAT1 regulates VSMC differentiation and calcification in as long noncoding RNA NEAT1 enhances phenotypic and osteogenic switching of vascular smooth muscle cells in atherosclerosis via scaffolding EZH2. *American Journal of Physiology-Cell Physiology*, 2024, **326**, C1721–C1734.
20. Zheng, F., Ye, C., Ge, R., et al., MiR-21-3p in extracellular vesicles from vascular fibroblasts of spontaneously hypertensive rat promotes proliferation and migration of vascular smooth muscle cells. *Life Sciences*, 2023, **330**, 122023.
21. Zhao, D., Zhuang, J., Wang, L., et al., Unveiling Key Biomarkers and Mechanisms in Septic Cardiomyopathy: A Comprehensive Transcriptome Analysis. *JIR*, 2024, **Volume 17**, 11451–11467.
22. Zhang, X., Zhang, X., Zhang, Y., et al., Abstract 10505: S100a12 Aggravates Acute Myocardial Infarction Injury Through Excessive Neutrophil Extracellular Trap Formation. *Circulation*, 2021, **144**.
23. Rao, R. S., Panbhukarasu, S., Waleed, M., et al., Neutrophil-Derived S100A8/A9 in Cardiovascular Disease and Beyond. *Curr.*

Pharmacol. Rep., 2023, **9**, 353–363.
24. Wu, L.-D., Li, F., Chen, J.-Y., Zhang, J., Qian, L.-L., and Wang, R.-X., Analysis of potential genetic biomarkers using machine learning methods and immune infiltration regulatory mechanisms underlying atrial fibrillation. *BMC Med Genomics*, 2022, **15**, 64.
25. He, Y., Jin, H., Zhao, J., et al., Single-cell transcriptomic analysis reveals differential cell subpopulations and distinct phenotype transition in normal and dissected ascending aorta. *Mol Med*, 2022, **28**, 158.
26. Zhangsun, Z., Dong, Y., Tang, J., et al., FPR1: A critical gatekeeper of the heart and brain. *Pharmacological Research*, 2024, **202**, 107125.
27. Lee, C., Han, J., and Jung, Y., Formyl peptide receptor 2 is an emerging modulator of inflammation in the liver. *Exp Mol Med*, 2023, **55**, 325–332.
28. Marshall, S. A., Qin, C. X., Jelinic, M., et al., The Novel Small-molecule Annexin-A1 Mimetic, Compound 17b, Elicits Vasoprotective Actions in Streptozotocin-induced Diabetic Mice. *IJMS*, 2020, **21**, 1384.
29. Studley, W. R., Lamanna, E., Martin, K. A., et al., The small-molecule formyl peptide receptor biased agonist, compound 17b, is a vasodilator and anti-inflammatory in mouse precision-cut lung slices. *British J Pharmacology*, 2024, **181**, 2287–2301.
30. Zhang, W., Zhang, J., Jiao, D., et al., Single-Cell RNA Sequencing Reveals a Unique Fibroblastic Subset and Immune Disorder in Lichen Sclerosus Urethral Stricture. *JIR*, 2024, **Volume 17**, 5327–5346.
31. Reglero-Real, N., Pérez-Gutiérrez, L., and Nourshargh, S., Endothelial cell autophagy keeps neutrophil trafficking under control. *Autophagy*, 2021, **17**, 4509–4511.
32. Zhou, C., Lin, Z., Cao, H., et al., Anxa1 in smooth muscle cells protects against acute aortic dissection. *Cardiovascular Research*, 2022, **118**, 1564–1582.
33. Filiberto, A. C., Ladd, Z., Leroy, V., et al., Resolution of inflammation via RvD1 / FPR2 signaling mitigates Nox2 activation and ferroptosis of macrophages in experimental abdominal aortic aneurysms. *The FASEB Journal*, 2022, **36**, e22579.
34. Schindler, L., Zwissler, L., Krammer, C., et al., Macrophage migration inhibitory factor inhibits neutrophil apoptosis by inducing cytokine release from mononuclear cells. *Journal of Leukocyte Biology*, 2021, **110**, 893–905.
35. Winneberger, J., Schöls, S., Lessmann, K., et al., Platelet endothelial cell adhesion molecule-1 is a gatekeeper of neutrophil transendothelial migration in ischemic stroke. *Brain, Behavior, and Immunity*, 2021, **93**, 277–287.
36. Abbott, R. J. M., Spendlove, I., Roversi, P., et al., Structural and Functional Characterization of a Novel T Cell Receptor Co-regulatory Protein Complex, CD97-CD55. *Journal of Biological Chemistry*, 2007, **282**, 22023–22032.
37. Yang, J., Song, X., Zhang, H., et al., Single-cell transcriptomic landscape deciphers novel olfactory neuroblastoma subtypes and intratumoral heterogeneity. Cancer Biology, 2023, January 25.
38. Wu, W., Bao, W., Chen, X., et al., Endothelial Gata6 deletion reduces monocyte recruitment and proinflammatory macrophage formation and attenuates atherosclerosis through Cmpk2-Nlrp3 pathways. *Redox Biology*, 2023, **64**, 102775.
39. Zhao, Y., Tan, M., Yin, Y., et al., Comprehensive macro and micro views on immune cells in ischemic heart disease. *Cell Proliferation*, 2024, **57**, e13725.
40. Wang, Z., Zhao, X., Zhao, G., et al., PRDM16 deficiency in vascular smooth muscle cells aggravates abdominal aortic aneurysm. *JCI Insight*, 2023, **8**, e167041.

41. Adachi, Y., Ueda, K., Nomura, S., et al., Beiging of perivascular adipose tissue regulates its inflammation and vascular remodeling. *Nat Commun*, 2022, **13**, 5117.
42. Sun, G., Li, K., Ping, J., et al., A single-cell transcriptomic atlas of the lungs of patients with pulmonary tuberculosis. In Review, 2024, March 19.
43. Zhang, S., Meng, Y., Zhou, L., et al., Targeting epigenetic regulators for inflammation: Mechanisms and intervention therapy. *MedComm*, 2022, **3**, e173.
44. Yu, A. M., Calvo, J. A., Muthupalani, S., and Samson, L. D., The Mbd4 DNA glycosylase protects mice from inflammation-driven colon cancer and tissue injury. *Oncotarget*, 2016, **7**, 28624–28636.
45. Li, S., He, R.-C., Wu, S.-G., et al., LncRNA PSMB8-AS1 Instigates Vascular Inflammation to Aggravate Atherosclerosis. *Circulation Research*, 2024, **134**, 60–80.
46. Wang, J., Farkas, C., Benyoucef, A., et al., Interplay between the EMT transcription factors ZEB1 and ZEB2 regulates hematopoietic stem and progenitor cell differentiation and hematopoietic lineage fidelity. *PLoS Biol*, (ed. Eaves, C. J.), 2021, **19**, e3001394.
47. Fu, M., Du, Y., Liu, F., et al., Prognostic value of KLFs family genes in renal clear cell carcinoma. *Sci Rep*, 2024, **14**, 20204.